



**Detecting boundary layer structure**

C. Milroy et al.

Title Page

Abstract

Introduction

Conclusions

References

Tables

Figures

I◀

▶I

◀

▶

Back

Close

Full Screen / Esc

Printer-friendly Version

Interactive Discussion



<sup>3</sup> Laboratoire des Sciences du Climat et de l'Environnement (LSCE) Unité mixte IPSL-UVSQ-CNRS-CEA, Orme des Merisiers, 91191 Gif-Sur-Yvette Cedex, France

<sup>4</sup> LMD, Laboratoire de Meteorologie Dynamique, Ecole Polytechnique, Palaiseau, France

\* now at: Max-Planck-Institute for Biogeochemistry, Hans-Knöll-Str. 10, 07745 Jena, Germany

Received: 12 November 2010 – Accepted: 10 December 2010 – Published: 21 January 2011

Correspondence to: C. Milroy (pricer@eircom.net)

Published by Copernicus Publications on behalf of the European Geosciences Union.

## Abstract

Twenty-one cases of boundary-layer (BL) structure were retrieved by three co-located remote sensors, one lidar (Leosphere ALS300) and two ceilometers (Vaisala CL31, Jenoptik CHM15K). Data were collected during the ICOS field campaign held at the GAW Atmospheric Station of Mace Head, Ireland, from 8 to 28 June 2009. The study is a two-step investigation of the BL structure based (i) on the intercomparison of backscatter profiles from the three laser sensors and (ii) on the comparison of the backscatter profiles with twenty-three radiosoundings performed during the period of 8 to 15 June 2009. The Temporal Height-Tracking (THT) algorithm was applied to the three sensors' backscatter profiles to retrieve the decoupled structure of the BL over Mace Head. The results of the intercomparisons are expressed in terms of the mean correlation coefficients, mean bias (difference between two sensors' detections), mean sigma (the standard deviation of the bias) and the consistency, i.e. the percentage of cases where the detections of the intercompared sensors were closer than 200 m. The ALS300-CHM15K comparison provided the most consistent retrievals amongst the three comparisons with, respectively, the 86.5% and 77.2% of the lower and upper layer detections closer than 200 m and with correlation coefficients equal to 0.88 and 0.83 at the lower and upper layer, respectively.

The lidar and ceilometers-detected BL heights were then compared to the temperature profiles retrieved by radiosoundings. The most consistent retrievals at the lower layer are from the ALS300 with the 75% of detections closer than 200 m to the radiosoundings' first temperature inversion. Despite the lower signal-to-noise ratio and  $R$ -value compared to the ALS300 and CHM15K, the CL31 is more consistent with the radiosoundings retrievals at the upper layer with 62.5% of detections closer than 200 m to the radiosoundings' second temperature inversion. The ALS300 has larger pulse-averaged power compared to the two ceilometers and better ability in detecting fine aerosol layers within the BL. The comparison of remote and in-situ data proved both the veracity of the inherent link between temperature and aerosol backscatter

## Detecting boundary layer structure

C. Milroy et al.

Title Page

Abstract

Introduction

Conclusions

References

Tables

Figures

◀

▶

◀

▶

Back

Close

Full Screen / Esc

Printer-friendly Version

Interactive Discussion



profiles, and the existence of possible limitations in using aerosols as a tracer to detect the BL structure.

## 1 Introduction

The planetary boundary layer (PBL) is the atmospheric region with the highest concentration of aerosols between the ground level and the free troposphere, and where aerosols experience turbulent mixing and are homogeneously distributed. The PBL is subject of study by both modellers and experimentalists using different approaches and definitions to characterize the structure of the boundary layer. One common point for most of the scientific community is to identify the PBL as the region where turbulent mixing of gas and aerosol occurs (Kunz et al., 2002; Serafin et al., 2010). High concentrations of aerosol can also be found higher up in the troposphere in correspondence of aerosol layers of volcanic or desert origin (Colette et al., 2008), whose particle concentration can often be higher than in the PBL. Atmospheric aerosols affect air quality and climate. In terms of air quality, aerosols influence human health, leading to increased mortality rates and deteriorated visibility (Salma et al. 2002; Cliff, 2005). Almost all anthropogenic and biogenic particles are created inside the PBL where they can stay for days. Aerosols can be dispersed out of the PBL during strong convection or temporary breaks of the capping temperature inversion (Mills et al., 1975; Halesa et al., 1972). Aerosols can be deposited to the ground by precipitation or by dry gravitational settling. Whilst the first process occurs on a time scale of minutes to hours, the second typically occurs on daily time scales, increasing with PBL height. Lifetime of pollutants within the PBL depends on both local and synoptic meteorological conditions and on the advected air mass. Aerosols can be generated locally or advected with the air mass which, depending on its origin, characterizes the aerosols population. The GAW atmospheric research station of Mace Head, Ireland, is located at the interface between the North-East Atlantic and Europe, thus enabling sampling of both the cleanest air entering into Europe along with some

## Detecting boundary layer structure

C. Milroy et al.

Title Page

Abstract

Introduction

Conclusions

References

Tables

Figures



Back

Close

Full Screen / Esc

Printer-friendly Version

Interactive Discussion



**Detecting boundary layer structure**

C. Milroy et al.

Title Page	
Abstract	Introduction
Conclusions	References
Tables	Figures
◀	▶
◀	▶
Back	Close
Full Screen / Esc	
Printer-friendly Version	
Interactive Discussion	



of the most polluted air being exported out of Europe into the North Atlantic (Suilou Huang et al., 2001; Derwent et al., 1994; McGovern et al., 1994). This study aims to provide quantitative information on the local boundary-layer (BL) height and structure detections as retrieved by one lidar and two ceilometers installed at the Mace Head station. Already other intercomparison studies of lidar and ceilometer retrievals of BL and cloud structures have shown improved efficiency in the detection techniques (Boers et al., 2000; Clothiaux et al., 2000; Kalb et al., 2004; Sicard et al., 2009). The method based on local maxima of the radiosounding-retrieved potential temperature vertical gradient is a convenient and widely used technique for both daytime and nighttime determination of the BL structure (Cramer 1972; Van Pul et al., 1994; De Wekker et al., 2004; Martucci et al., 2007). For the cases that are presented in this study, the measurements have been carried out during the period from 8 to 28 June 2009, in the frame of the ICOS (Integrated Carbon Observation System) field campaign at Mace Head. ICOS is a new European Research Infrastructure for quantifying and understanding the greenhouse balance of the European continent and of adjacent regions (<http://www.icos-infrastructure.eu/>). During the preparatory phase from 2008 until 2011, the building of the central facilities is initiated, and the project is technically developed to the level of a demonstration year of full operation, but with a reduced number of observational sites. As part of the field campaign, one lidar and two ceilometers have been deployed for BL monitoring: the Leosphere ALS300, the Jenoptik CHM15K and Vaisala CL31, respectively. Within the specific operating vertical range of each instrument, the lidar and the ceilometers provided the backscatter profiles used to retrieve the BL structure. The Temporal Height-Tracking (THT) algorithm (Martucci et al., 2010a,b) has been applied to the three sensors' output data to retrieve the two-layer structure of the local BL. The two layers are defined as a lower, well mixed surface layer and a decoupled layer occupying the region below the free troposphere, i.e. the decoupled residual (nocturnal) or convective (diurnal) layer. Twenty-five meteorological sondes (Vaisala RS92-SGPD) were made available for the ICOS Mace Head Campaign to provide tropospheric in-situ measured profiling

above Mace Head. The daily timetable was with four ascents at 05:15, 11:15, 17:15 and 23:15 UTC (same as local time). Total of 23 sondes have been successfully launched during the first week of campaign, i.e. 8–15 June. An independent algorithm was developed to retrieve the inversions in the radiosoundings-detected temperature profiles and to compare them to the lidar and ceilometer-detected BL structure allowing independent comparison of the 2-layered structure of the BL.

## 2 Site overview and local boundary-layer structure

### 2.1 The site

Located on the west coast of Ireland (53.20° N, 9.54° W), the Atmospheric Research Station of Mace Head, Carna, County Galway is unique in Europe: its position offers westerly exposure to the North Atlantic Ocean through the *clean sector* (190°–300° N) and the opportunity to study atmospheric composition under northern hemispheric background conditions as well as European continental emissions when the winds favour transport from that region. The site is located in the path of the mid-latitude cyclones which frequently traverse the North Atlantic. The sensors were located 300 m from the shore line on a gently-sloping hill (4 degrees incline).

### 2.2 Boundary layer structure

Characteristic of this region and related to warm waters, the marine boundary layer is typically two-layered with a surface mixed layer (SML) and a decoupled residual or convective layer (DRCL) above which is the free troposphere (Stull, 1988; Kunz et al., 2002). The site is exposed to both polluted and clean air masses, with aerosol load changing accordingly to the air characteristic. Changes in air masses (temperature and aerosol load) directly affect the BL's depth and the aerosol concentration; BL is normally deeper during polluted periods and shallower when air masses carry clean

## Detecting boundary layer structure

C. Milroy et al.

Title Page

Abstract

Introduction

Conclusions

References

Tables

Figures

◀

▶

◀

▶

Back

Close

Full Screen / Esc

Printer-friendly Version

Interactive Discussion



cold marine air. From studies performed during extended periods of BL monitoring (Dall'Osto et al., 2010; Martucci and O'Dowd, 2009) it turned out that the distance between SML and DRCL remains fairly constant during different air masses showing that the BL decoupling over Mace Head is independent on the air mass characteristic.

### 3 The laser sensors

#### 3.1 Leosphere ALS300

The ALS300 uses a tripled pulse laser source Nd:YAG at 355 nm wavelength with an energy of 16 mJ and pulse repetition frequency of 20 Hz. Both analogue and photon counting detection is available. The Lidar system provides a real-time measurement, of backscattering and extinction coefficients, Aerosol Optical Depth (AOD), automatic detection of the planetary boundary layer height and clouds base and top from 75 m (200 m full overlap) up to 20 km, together with scanning capabilities and polarization channel with a raw resolution of 1.5 m.

#### 3.2 Jenoptik CHM15K

The CHM15K ceilometer (Flentje et al., 2010; Martucci et al., 2010a) measures atmospheric target backscatter profiles over the nominal range 0.03–15 km with first overlap point at 30 m (1500 full overlap). In the operating range of 15 km it can reliably detect lower cloud layers as well as cirrus clouds although the latter can be hidden in the noisy component of the signal at these high ranges. The highest vertical resolution at which the instrument can work is 15 m with measured full vertical profiles of aerosol backscatter and detected cloud height, boundary layer height and visibility values. The measuring principle is LIDAR-based with photon counting detection system and solid-state Nd:YAG laser source emitting at the 1064 nm wavelength with undeclared manufacturing accuracy.

## Detecting boundary layer structure

C. Milroy et al.

Title Page

Abstract

Introduction

Conclusions

References

Tables

Figures

◀

▶

◀

▶

Back

Close

Full Screen / Esc

Printer-friendly Version

Interactive Discussion



### 3.3 Vaisala CL31

The enhanced single lens technology applied to the CL31 ensures realistic data recording over the nominal range 0–7.5 km with first point of overlap at 0 m (full overlap nearly at the first range gate, Munkel et al., 2007). The good quality of the received signal is made possible by the strong and stable signal over the whole measurement range. Although the single lens technology is meant to provide reliability during precipitation, the receiving system becomes saturated very quickly during precipitation events. The laser is an InGasAs diode emitting at the 910 nm wavelength with a manufacturing estimated accuracy of  $\pm 5$  m (against hard target) equal to the highest vertical resolution  $\Delta z = 5$  m.

### 4 Methodology and data analysis

The power of the lidar signal,  $P(h)$ , backscattered by an atmospheric layer of thickness  $\Delta h$  (range gate) centred at altitude  $h$  can be expressed in the form (Weitkamp, 2005):

$$P(h) = P_L K O(h) \frac{A}{h^2} \Delta h \beta(h) T^2(h) + B, \quad (1)$$

$P_L$  is the emitted optical power,  $K$  the overall optical efficiency of the instrument,  $O(h)$  is the overlap function,  $A$  the receiver area and  $T(h) = \exp \left\{ -2 \int_0^h \alpha(h') dh' \right\}$  is the round-trip transmission factor. Variables  $\alpha$  and  $\beta$  are respectively the extinction (in  $[m^{-1}]$ ) and the volume backscattering (in  $[sr^{-1} m^{-1}]$ ) coefficients. The last term  $B$  is the sum of the electronic and optical background noise. The coefficients  $\alpha$  and  $\beta$  can be written as the combination of their aerosol and molecular components, i.e.  $\alpha = \alpha_{aer} + \alpha_{mol}$  and  $\beta = \beta_{aer} + \beta_{mol}$ . For the utilized wavelengths (355 nm, 910 nm and 1064 nm) the relation  $\alpha_{aer} \cdot \beta_{aer} \gg \alpha_{mol} \cdot \beta_{mol}$  can be applied. This assumption applies also to the gradient of the received power since the vertical changes in

## Detecting boundary layer structure

C. Milroy et al.

Title Page

Abstract

Introduction

Conclusions

References

Tables

Figures

◀

▶

◀

▶

Back

Close

Full Screen / Esc

Printer-friendly Version

Interactive Discussion



aerosol/hydrometeor concentration dominate the received signal at both long ( $\lambda \approx 1 \mu\text{m}$ ) and short wavelengths ( $\lambda \approx 0.35 \mu\text{m}$ ). The extinction and the backscatter coefficients can then be written as  $\alpha \approx \alpha_{\text{aer}}$  and  $\beta \approx \beta_{\text{aer}}$ , respectively.

The attenuated atmospheric volume backscatter coefficient ( $\beta^{\text{att}}$ ) is computed as,

$$\beta^{\text{att}}(h) = [P(h) - B]h^2 / P_L K A \Delta h \quad (2)$$

Backscatter profiles from the three sensors are used as input to the THT scheme (Martucci et al., 2010a, b) with 5-min and 30-m temporal and vertical resolution, respectively. The adopted THT algorithm is based on the information on the mutual positions of the local minima in the  $\beta^{\text{att}}$  vertical profile and its vertical gradient (GS, Gradient Signal) where the gradient applies to the natural logarithm of  $\beta^{\text{att}}$ . For a timeseries of  $N$  profiles the  $i$ th gradient profile has the form:

$$\text{GS}_i(h) = \frac{d}{dh} \log(\beta_i^{\text{att}}(h)) = \frac{d}{dh} \log(\beta_i(h)) - 2\alpha_i(h) \quad (3)$$

The index  $i$  goes from 1 to the end of the dataset and  $N$  depends on the dataset duration and the sampling rate (5 min for this study). The algorithm computes the mean  $\overline{\text{GS}}$  and  $\overline{\beta^{\text{att}}}$  values from single  $\text{GS}_i$  and  $\beta_i^{\text{att}}$  profiles averaged over 10-min (i.e. over 2 profiles). The mean value between the heights of the two minima is a reference height,  $h_{\text{ref}}$  used to “track” the successive BL height determinations at each  $i$ -step (new  $h_{\text{ref}}$  heights are calculated every 10 min and used to determine the consecutive BL heights). Radiosounding readings of temperature profiles and their calculated temperature profile gradients are processed in order to return two inversions which represent the top of SML and DRCL. Using the radiosoundings as independent source of height values for the BL’s two layers, comparisons are made between these values and each of the sensors’ two layers retrieved by the THT algorithm.

## Detecting boundary layer structure

C. Milroy et al.

Title Page

Abstract

Introduction

Conclusions

References

Tables

Figures

◀

▶

◀

▶

Back

Close

Full Screen / Esc

Printer-friendly Version

Interactive Discussion



## 5 Results

### 5.1 Lidar-ceilometers intercomparison

Vertical backscatter profiles from ceilometers and lidar have been processed using the THT technique to retrieve the two-layered structure of the BL. Figures 1 and 2 show examples of the time-height cross sections of the atmospheric attenuated backscatter retrieved by the ALS300 (top), CHM15K (middle) and CL31 (bottom) in the time interval between 00:00 to 24:00 UTC on 15 and 20 June 2009, respectively. White circles and triangles superimposed to the backscatter timeseries represent the SML and DRCL detections, respectively. Resulting BL-structures from the ALS300, CHM15K and CL31 have been intercompared at each time step for all cases. The intercomparison's output in terms of SML and DRCL detections retrieved by the THT algorithm can vary significantly from case to case depending on meteorological conditions and on the different instrumental skills. The cases selected for the intercomparison match the following criteria: no or negligible precipitation occurring during the measurements; no or negligible patches of low fog causing the laser beam to get extinct below the actual BL height; the sensors operated with no technical difficulties; time of measurements is synchronized for all sensors. Table 1 summarizes the mean statistical properties of all intercomparisons for each detected layer, SML and DRCL. For each  $Y$  vs.  $X$  device the mean statistical variables describing their comparison are: the correlation coefficient,  $R$ ; the *bias*, i.e. the mean absolute value of the difference between  $Y$  and  $X$ -detections; *sigma*, i.e. the standard deviation of the  $Y - X$  differences; the *consistency*, i.e. the percentage of  $X$  and  $Y$ -detections closer than 200 m, i.e.  $\text{abs}(Y - X) \leq 200$  m.

The two cases in Figs. 1 and 2 show a cloud-free and a cloudy BL daily development on 15 and 20 June, respectively. During 15 June 2009 the SML and DRCL detections experienced moderate variability especially during the central hours of the day, from 11:00 to 20:00 UTC. The higher SML variability on the 15th compared to the 20th is mainly due to the clear sky conditions that enhanced the convection in the lower layer. Similarly, the DRCL on the 15th had larger height-fluctuations (top and middle panel)

## Detecting boundary layer structure

C. Milroy et al.

Title Page

Abstract

Introduction

Conclusions

References

Tables

Figures

◀

▶

◀

▶

Back

Close

Full Screen / Esc

Printer-friendly Version

Interactive Discussion



probably due to formation and breakdown of thermals, transporting aerosols in updrafts and downdrafts at the top of the BL.

On 20 June, precipitation occurred in two short events at the beginning and at the end of the day; a thin deck of stratus cloud topping the SML formed since the early morning (~02:30 UTC) and remained between 1000 and 500 m until mid-afternoon (16:00 UTC) with only one short break in the cloud cover before noon. The detected BL presented a stratiform-driven structure with slowly-changing SML height and a hardly detectable DRCL. In the bottom panel the DRCL was not detected by the CL31 due to the almost complete signal extinction through the cloud layer. That was not the case for the ALS300 which could penetrate the cloud layer using larger power pulse and detect the DRCL above. In the middle panel, the CHM15K retrievals of the DRCL match very closely those of the ALS300.

Figures 3 and 4 show the linear correlations of the three-instrument intercomparison for the SML and DRCL detections on 15 and 20 June. The DRCL detections are shown only for the case of 15 June due to too few DRCL detections by the CL31 on 20 June. The different meteorological conditions on the 15th and the 20th lead to different detection conditions for the lidar and the two ceilometers: the missing DRCL detection on the 20th is caused by both the presence of the deck of stratus cloud and the lower pulse power of the CL31 device compared to the other two devices. For SML detection, higher correlations are obtained for the case in which the SML matches the stratus cloud. The strong echo from the cloud is detected clearly by the three sensors and the passage from the SML to the DRCL is well defined reducing significantly the THT uncertainty in assigning the SML height. Not forgetting the different meteorological conditions, the DRCL detection on the 15th shows better matching for the ALS300-CHM15K comparison than for the others. This is more generally confirmed by the statistical values reported in Table 1: for the ALS300-CHM15K comparison the correlation coefficients  $R$  at the SML and DRCL levels are 0.88 and 0.83, respectively, with the most consistent retrievals amongst the three intercomparisons (86.5% and 77.2% for SML and DRCL, respectively).

## Detecting boundary layer structure

C. Milroy et al.

Title Page

Abstract

Introduction

Conclusions

References

Tables

Figures

◀

▶

◀

▶

Back

Close

Full Screen / Esc

Printer-friendly Version

Interactive Discussion



## 5.2 In-situ versus remote sensing measurements

The THT-processed backscatter data have been compared to the radiosoundings, Table 2 details the data being used for the comparisons. Maxima in the vertical gradient of the temperature profile of the radiosoundings were used to determine SML and DRCL layers which then could be compared to the sensors' retrievals. Lidar and ceilometers data have not been used in three cases due to rain occurring during the radiosounding ascents. CHM15K data were not available on the 9th; data from the CL31 and ALS300 recorded on the 9th were not used then for the correlations (data from the 9th retrieved by the CL31 and ALS300 will be discussed separately in Sect. 5.3). Due to the limited number of available data points for the comparison, the obtained correlation coefficients  $R$  are highly sensitive to the single datum; since the comparisons depend on a number of variables including meteorological conditions (cloud cover, fog and precipitation) and the aerosol load, an accurate analysis of all cases is performed in order to interpret correctly the obtained correlations. Table 3, identically to Table 1, summarizes the *bias*, *sigma* and *consistency* of the comparisons of each instrument versus the radiosounding (RS) at the SML and DRCL levels.

### 5.2.1 ALS300 vs. RS

Figure 5 shows the linear correlations between ALS300 and RS retrievals for the SML and DRCL detections. The ALS300-detected SML values closely distribute around the 1:1 line with high correlation coefficient equal to 0.911. Detections of both layers, the SML and DRCL, result very accurate especially compared, *ceteris paribus*, to the other two remote sensors. The better performance of the ALS300 (and then of the THT applied to the ALS300 signal) in retrieving closer SML and DRCL detections to the RS main temperature inversions is principally due to the large pulse power and the high SNR. The two parameters imply high skill in detecting fine aerosol layers within the BL and allow clear identification of gradients along the backscatter profiles. However, this may turn into negative consequence when using a gradient-based algorithm such as THT since higher number of aerosol layers (and then gradients) within the SML

## Detecting boundary layer structure

C. Milroy et al.

Title Page

Abstract

Introduction

Conclusions

References

Tables

Figures

◀

▶

◀

▶

Back

Close

Full Screen / Esc

Printer-friendly Version

Interactive Discussion



**Detecting boundary layer structure**

C. Milroy et al.

Title Page

Abstract

Introduction

Conclusions

References

Tables

Figures

◀

▶

◀

▶

Back

Close

Full Screen / Esc

Printer-friendly Version

Interactive Discussion



or DRCL can lead to increase the uncertainty when comparing SML or DRCL to the RS single-detection. The fact that the DRCL detections have comparable and slightly higher correlation coefficient (0.922) with respect to the SML's confirms that the interface with the free troposphere is unambiguously detected and not confused by the algorithm with other internal layers. The number of data points is 16 for the SML and 13 for the DRCL; the statistical parameters reported in Table 3 show that the ALS300 can assure the most consistent SML and DRCL retrievals with 75% and 61.5% of detections closer than 200 m to the RS retrievals, respectively. An analysis of the ALS300 backscatter profiles shows that the instrument can deliver more accurate information on the fine BL structure than the two ceilometers based on the higher SNR in the first 5 km.

The closest ALS300-RS detection of the SML was 27.5 m which occurred on 15 June at 05:05 UTC; the lower overlap height allowed the ALS300 to pick up the low level inversion delimiting the upper boundary of the developing diurnal SML on that day. The THT-detected heights from the ALS300, CL31 and CHM15K backscatter profiles have been 312.5 m, 545 m and 592 m, respectively, whilst the actual RS showed the main inversion at 340 m on the 15th. The largest difference at the SML level was 437.5 m which occurred on 14 June at 05:05 UTC with high discrepancies occurring throughout the entire day. As for the CHM15K and CL31 during the 14th, the convective conditions affected the results of the comparison.

The DRCL comparison counts 13 samples, the closest ALS300-RS detection of the DRCL was 6.5 m which occurred on 13 June at 06:05 UTC when the detected DRCL depth was 1400 m. The largest discrepancy between the in-situ and the ALS300 retrievals occurred on 11 June at 11:15 UTC with a value of 421.5 m when the DRCL depth was only 75 m, i.e. only 5 percent the depth on the 13th. This supports the hypothesis that shallower DRCL can make THT's detection of the BL height uncertain. As it will be shown in the next two sections, the application of the THT algorithm to the ALS300 backscatter profiles returned better results than for the other sensors resulting in closer detections to the RS retrievals even in conditions with shallow DRCL.

## 5.2.2 CHM15K vs. RS

Figure 6 shows the linear correlations between CHM15K and the RS retrievals of the SML and DRCL heights. Each RS data-point corresponds to an ascent's duration of about 10–15 min to reach the height of 3 km. The ascent's duration determines also the time of average of the backscatter profile to be compared with the RS temperature vertical profile. Both the SML and DRCL show good correspondence with the radiosoundings demonstrating that the decoupled aerosol-based SML and DRCL structure corresponds well to the retrieved temperature structure. The CHM15K-RS comparison counts 17 samples for the SML and 15 for the DRCL (out of 23). The data summarized in Table 3 report the values of  $R$ ,  $bias$ , and  $sigma$  (0.88, 177.2, and 191.6, respectively) and the percentage of consistent retrievals in the comparison, 64.7%. An indication of the over- or under-estimation of the SML height is provided by the slope of the linear fit equal to 0.91 that, in combination with the small intercept (42 m), suggests a slight underestimation of the temperature-retrieved SML height by the CHM15K.

The smallest difference between the CHM15K's SML reading and the radiosoundings first inversion is 13 m measured on 12 June at 17:15 UTC. For the SML detections, all readings on the 12th showed only minor differences between the CHM15K's and radiosoundings' reading. During periods of clear inversions with minimal multiple inversions the THT application to the CHM15K's backscatter profiles matches closer the radiosoundings retrievals. The largest difference between the CHM15K- and RS-detected SML heights has been 270 m measured on 13 June at 17:35 UTC and readings throughout the day had largely differed from radiosoundings retrievals. The lidar-retrieved BL structure on the 13th has been affected by the high-frequency fluctuations of both the SML and DRCL due to prolonged convection occurring in the almost cloud-free day conditions.

The comparison between the CHM15K and the radiosoundings for the DRCL detections is based on 15 samples with average RS-detected DRCL depth of 800 m. The closest DRCL detection between CHM15K and RS is 40.5 m retrieved on 14 June

### Detecting boundary layer structure

C. Milroy et al.

Title Page

Abstract

Introduction

Conclusions

References

Tables

Figures

◀

▶

◀

▶

Back

Close

Full Screen / Esc

Printer-friendly Version

Interactive Discussion



**Detecting boundary layer structure**

C. Milroy et al.

Title Page	
Abstract	Introduction
Conclusions	References
Tables	Figures
◀	▶
◀	▶
Back	Close
Full Screen / Esc	
Printer-friendly Version	
Interactive Discussion	

at 11:00 UTC. The remote and in-situ measurements on the 14th returned close DRCL values also for the other three ascents. For the 11:00 UTC ascent the RS-detected layer between first and second main temperature inversion was 1271 m (SML at 953 m and DRCL at 2224 m). Observations showed that when the distance between first and second temperature inversion increases (net decoupling), the CHM15K retrievals of the DRCL become closer to the RS detections. High-frequency fluctuations of the DRCL and SML can occur during enhanced and prolonged convective conditions; in such conditions the temperature inversions are generally less pronounced and the retrievals using RS less accurate. Also, rapidly-fluctuating SML and DRCL upper boundaries are hard to detect using lidar and ceilometer especially when the DRCL is shallow and the instrument vertical resolution can not resolve properly the weak gradients. When this happens, the comparison between in-situ and remotely sensed detections becomes very uncertain. The largest discrepancy between the CHM15K and RS reading of the DRCL was 279.5 m and occurred on 10 June at 23:15 UTC; the comparisons throughout the entire day showed larger differences compared to other cases. 10 and 11 June had generally shallower DRCL, e.g. 79 m on the 10th at 23:15 UTC. The very thin DRCL corresponded to a less defined decoupling in the temperature profile as well, confirming that the comparison between lidar and RS improves when temperature inversions are stronger and the two-layer BL structure is neatly decoupled.

**5.2.3 CL31 vs. RS**

Figure 7 shows the linear correlations between CL31 and RS retrievals for the SML and DRCL detections. The SML and DRCL comparisons have linear correlation coefficients 0.744 and 0.605, respectively. The comparison for the SML has higher correlation coefficient than the DRCL's. The worse DRCL detections are due to the rapidly decreasing SNR above 1 km which makes the detection of the aerosol layers by the CL31 more difficult in daylight. The number of DRCL detections (8) is smaller than the one for CHM15K and ALS300 and this is due to the higher SNR of the other two devices. Three days (12 data points) were not available for the comparison: on the



## Detecting boundary layer structure

C. Milroy et al.

Title Page

Abstract

Introduction

Conclusions

References

Tables

Figures

◀

▶

◀

▶

Back

Close

Full Screen / Esc

Printer-friendly Version

Interactive Discussion



10th and 11th data were not available for technical reasons and on the 14th the CL31 did not detect the DRCL at the time of the 4 ascents. Nevertheless, data from Table 3 highlight that more DRCL than SML detections are consistent with the RS. Despite the rapidly decreasing SNR, the *bias* shows values of 218.2 m for the SML and only 143.4 m for the DRCL leading to a *consistency* value of only 36.4% at the SML and as high as 62.5% at the DRCL level (an interpretation of this result is provided in the Conclusions).

The SML comparison is based on 11 samples, the smallest difference between the CL31 and the radiosoundings is 41 m, measured on 12 June at 11:15 UTC. Similar to the CHM15K when the inversions are sharp and the BL decoupling is neat the THT application to the backscatter profiles provides closer values to the RS retrievals. The most divergent CL31 and RS detection at the SML was 338.5 m, measured on 13 June at 06:05 UTC with large discrepancies detected throughout the entire day. As described for the previous comparison, the large discrepancies obtained on this day between remote and in-situ detections likely depend on the persisting convective conditions that occurred during the central hours of the day.

The DRCL counted on 8 samples, the closest CL31 and RS detection of the DRCL was 21 m, measured on 13 June at 06:05 UTC with all DRCL detections by the CL31 being very close to the temperature inversions during the entire day. The largest discrepancy at the DRCL level was 306 m, measured on 12 June at 11:15 UTC. Nonetheless, a missing or incorrect retrieval of the DRCL due to low SNR does not necessarily correspond to an incorrect SML retrieval, and in fact on the same day at the same time the CL31-retrieved SML differs from the radiosounding only by 66 m.

### 5.3 9 June 2009: undetected temperature inversion

In this section the case of 9 June is analysed for the ALS300 and CL31 outputs. The authors of this paper agree on the definition of the boundary-layer height as the top of the atmospheric region where the surface friction influences the aerosols turbulent mixing determines the homogeneous distribution of constituents. The idea

**Detecting boundary layer structure**

C. Milroy et al.

[Title Page](#)[Abstract](#)[Introduction](#)[Conclusions](#)[References](#)[Tables](#)[Figures](#)[I◀](#)[▶I](#)[◀](#)[▶](#)[Back](#)[Close](#)[Full Screen / Esc](#)[Printer-friendly Version](#)[Interactive Discussion](#)

that aerosol are the optimal tracer to detect the structure and the height of the BL is somehow controversial and is subject to different opinions within the scientific community (Pearson et al., 2010). Indeed, the case of 9 June demonstrates that some limitation with this definition may occur, especially when dealing with the concept of turbulence and temperature inversions as the region where turbulence breaks down. Based on this assumption the level where the aerosol concentration abruptly decreases should always match the level at which the main temperature inversion occurs. On 9 June at 05:15 UTC (sunrise at 04:12 UTC) the CL31 and the ALS300 clearly detected the top of the local DRCL in correspondence of a capping stratus cloud at 1670 m and 1500 m, respectively. No decoupled structure was observed at the time the observations were performed with the aerosols homogeneously distributed over the DRCL single-layer. On the other hand, the radiosoundings showed a clear low-level inversion at 315 m likely corresponding to the SML and a second inversion further up at 1720 m matching the DRCL. Neither the CL31 nor the ALS300 detected any aerosol layer matching the lower main inversion. Details of the backscatter and temperature profiles are shown in Fig. 8. Solid and dashed horizontal lines in the figure show the altitude of the two temperature inversions.

The radiosounding temperature profile (bottom-left) shows an inversion at 315 m likely capping the SML; the vertical gradient (bottom-right) shows that the lower inversion is the main along the profile up to 2000 m, a secondary inversion occurs at 1720 m. The CL31 backscatter profile (middle-left) and its gradient (middle-right) present no aerosol layer at the level where the main inversion occurs only detecting the DRCL at 1670 m.

The fact that neither the ALS300 nor the CL31 detected the decoupled structure of the BL on the morning of the 9th shows that limitations may exist when applying general algorithms based on the aerosol backscatter vertical gradient.

## 5.4 12 June 2009: detected temperature inversions

The case presented in Fig. 9 shows an example of good matching of the detected BL structure by remote and in-situ measurements. On 12 June 2009 a stratiform cloud was capping the BL above Mace Head at 11:15 UTC; the atmospheric column below the cloud base appeared to be well mixed, as it demonstrates the almost adiabatic temperature profiles in the bottom-left panel of Fig. 9 below the BL top (1210 m) with very weak secondary maximum matching the temperature inversion at 510 m. Differently from the previous case, all remote sensing data were available on the 12th. The three sensors show homogeneous, well-mixed layer below the cloud base with very weak decoupling at the heights 530 m, 570 m and 560 m for ALS300, CHM15K and CL31, respectively. In this case the aerosol proves to be a good tracer for the BL structure detection even when the backscatter gradients are poorly defined in the profiles of all three remote sensors.

## 6 Conclusions

This study is a two-step investigation of the BL structure over Mace Head, Ireland: (i) intercomparison of three remote backscatter sensors and (ii) comparison of the backscatter profiles with the radiosounding-retrieved temperature profiles. During the first part of the study three remote sensors have been intercompared, an elastic backscatter lidar (Leosphere ALS300) and two ceilometers (Jenoptik CHM15K and Vaisala CL31), the measurements have been performed during the ICOS field campaign from 8 to 28 June 2009. The Temporal Height-Tracking algorithm (Martucci et al., 2010a, b) has been applied to the backscatter profiles of the three sensors to retrieve the decoupled structure of the BL. The description of the BL is based on a two-layer BL with a surface mixed layer and a decoupled residual (nocturnal) or convective (diurnal) layer retrieved by the THT algorithm. The 21 timeseries (daily comparisons from 8 to 28 June) of SML and DRCL heights obtained by applying the THT to the three remote sensors backscatter signals have been intercompared. As summarized in

## Detecting boundary layer structure

C. Milroy et al.

Title Page

Abstract

Introduction

Conclusions

References

Tables

Figures

◀

▶

◀

▶

Back

Close

Full Screen / Esc

Printer-friendly Version

Interactive Discussion



## Detecting boundary layer structure

C. Milroy et al.

Title Page

Abstract

Introduction

Conclusions

References

Tables

Figures

◀

▶

◀

▶

Back

Close

Full Screen / Esc

Printer-friendly Version

Interactive Discussion



Table 1, the intercomparison showed that the ALS300 lidar and the CHM15K ceilometer returned closest detections of both the SML and DRCL heights with respectively the 86.5% and 77.2% of consistent detections, i.e. detections closer than 200 m. The SML detections by the three sensors registered higher correlation coefficients and consistency values than the DRCL ones. The interpretation of this result is in the difference of SNR amongst the three sensors: at the SML level the SNR is normally greater than 1 for all three instruments, but at the DRCL level only the ALS300 can provide signal with  $SNR > 1$ . The different SNR of the three sensors' signals cause the intercomparison to fail more often at the DRCL than at the SML. Moreover, the larger lidar pulse power of the ALS300 and CH15K determine better skills for these two devices in penetrating thin clouds and retrieve aerosol layers above it. On the other hand, the fact that the ALS300 has higher sensitivity to fine aerosol layers within the BL may enhance the disagreement with the other backscatter retrievals. The same problem arises when the ALS300 is compared to the single SML detection by the radiosoundings. As general outcome of the intercomparison the mean correlation coefficients over all the collected cases were  $R=0.88$ ,  $0.82$  and  $0.76$  for ALS300 vs. CHM15K, CHM15K vs. CL31 and ALS300 vs. CL31, respectively.

The second part of the study consists in the comparison of the obtained lidar and ceilometers SML and DRCL detections with the first two main inversions in the temperature profile retrieved by the radiosoundings. Dynamics which make the comparison more difficult are (i) enhanced convection leading to high-frequency variations of the SML and DRCL heights, (ii) shallow DRCL, and (iii) weak temperature inversions. Temporal and vertical resolutions of lidar and ceilometers are, as well as the SNR, key parameters that determine the accuracy of the retrievals. The observations demonstrated that a decoupled structure of the BL exists over Mace Head with distinct SML and DRCL, but the detections are best performed in cases where there is well-defined temperature inversion; remote-to-insitu linear correlations obtained for such these cases are in general very high. The  $R$ -values for the remote-to-insitu SML comparisons were  $0.91$ ,  $0.74$  and  $0.88$  for the ALS300, CL31 and CHM15K,

**Detecting boundary layer structure**

C. Milroy et al.

Title Page

Abstract

Introduction

Conclusions

References

Tables

Figures

◀

▶

◀

▶

Back

Close

Full Screen / Esc

Printer-friendly Version

Interactive Discussion



respectively. Similarly, the  $R$  values for the DRCL comparisons were 0.92, 0.61 and 0.81 for the ALS300, CL31 and CHM15K, respectively. Table 3 additionally shows that the most consistent retrievals at the SML level are those from the ALS300 with the 75% of detections closer than 200 m to the RS's first temperature inversion. Despite the lower SNR and  $R$ -value compared to the ALS300 and CHM15K, the CL31 is more consistent with the RS retrievals of the DRCL with 62.5% of detections closer than 200 m to the RS's second temperature inversion. However Table 3 shows the number of samples is significantly lower, the CL31 having samples ~60% of CHM15K and ALS300. This means that in 5 cases out of 23 the CL31 is getting DRCL detections closer than 200 m to the RS's.

The cases of 9 and 12 June have been discussed separately as example of cases in which the definition of a boundary layer based on the aerosol temporal and vertical distribution fails and succeeds, respectively. The case of the 9th is peculiar for the missing detection by the ALS300 and CL31 of any significant gradient in the backscatter profile at the level of the SML, whilst the temperature profiles indicate a clear inversion at 315 m likely matching the SML. On the other hand, the case of the 12th shows an example in which the use of aerosol as a tracer to determine the structure of the boundary layer provide faithful detections compared to the RS.

**Appendix A****List of acronyms**

PBL, Planetary Boundary Layer; BL, Boundary Layer; SML, Surface Mixed Layer; FOV, Field Of View; GS, Gradient Signal; RCS, Range-Corrected Signal; SNR, Signal-to-Noise Ratio; UTC, Universal Time Coordinated; PBL, Planetary Boundary Layer; BL, Boundary Layer; SML, Surface Mixed Layer; DRCL, Decoupled Residual or Convective Layer; FOV, Field Of View; GS, Gradient Signal; RCS, Range-Corrected Signal; SNR, Signal-to-Noise Ratio; UTC, Universal Time Coordinated.

*Acknowledgements.* The authors acknowledge the ICOS Preparatory Phase project for funding the radiosoundings. They are grateful to Jenny Hanafin, Cyrille Vuillemin, Benoit Wastine, Gionata Biavati and Guillaume Gorju for their important contribution in carrying out the radiosoundings and helping to set up optimally the instrumentation deployed during the field campaign.

## References

- Boers, R., Russchenberg, H., Erkelens, J., and Venema, V.: Ground-based remote sensing of stratocumulus properties during CLARA, 1996, *J. Appl. Meteorol.*, 39, 169–181, 2000.
- Clothiaux, E. E., Ackerman, T. P., Mace, G. G., Moran, K. P., Marchand, R. T., Miller, M. A., and Martner, B. E.: Objective determination of cloud heights and radar reflectivities using a combination of active remote sensors at the ARM CART sites, *J. Appl. Meteorol.*, 39, 645–665, 2000.
- Colette, A., Menut, L., Haeffelin, M., and Morille, Y.: Impact of the transport of aerosols from the free troposphere towards the boundary layer on the air quality in the Paris area, *Atmos. Environ.*, 42, 390–402, 2008.
- Cramer, O. P.: Potential temperature analysis for mountainous terrain, *J. Appl. Meteorol.*, 11, 44–50, 1972.
- Dall'Osto, M., Ceburnis, D., Martucci, G., Bialek, J., Dupuy, R., Jennings, S. G., Berresheim, H., Wenger, J., Healy, R., Facchini, M. C., Rinaldi, M., Giulianelli, L., Finessi, E., Worsnop, D., Ehn, M., Mikkilä, J., Kulmala, M., and O'Dowd, C. D.: Aerosol properties associated with air masses arriving into the North East Atlantic during the 2008 Mace Head EUCAARI intensive observing period: an overview, *Atmos. Chem. Phys.*, 10, 8413–8435, doi:10.5194/acp-10-8413-2010, 2010.
- Davidson, C. I., Phalen, R. F., and Solomon, P. A.: Airborne particulate matter and human health: a review, *Aerosol Sci. Tech.*, 39, 737–749, 2005.
- Derwent, R. G., Simmonds, P. G., and Collins, W. J.: Ozone and carbon monoxide measurements at a remote maritime location, mace head, Ireland, from 1990 to 1992, *Atmos. Environ.*, 28, 2623–2637, 1994.

## Detecting boundary layer structure

C. Milroy et al.

Title Page

Abstract

Introduction

Conclusions

References

Tables

Figures

◀

▶

◀

▶

Back

Close

Full Screen / Esc

Printer-friendly Version

Interactive Discussion



**Detecting boundary layer structure**

C. Milroy et al.

Title Page

Abstract

Introduction

Conclusions

References

Tables

Figures

◀

▶

◀

▶

Back

Close

Full Screen / Esc

Printer-friendly Version

Interactive Discussion



- De Wekker, S. F. J., Kossmann, M., and Fielder, F.: Observations of daytime mixed layer heights over mountainous terrain during the TRACT field campaign. Proc. 12th Symp. on Boundary Layers and Turbulence, Vancouver, BC, Canada, Am. Meteor. Soc., 498–499, 1997.
- 5 Flentje, H., Heese, B., Reichardt, J., and Thomas, W.: Aerosol profiling using the ceilometer network of the German Meteorological Service, Atmos. Meas. Tech. Discuss., 3, 3643–3673, doi:10.5194/amtd-3-3643-2010, 2010.
- Hales, J. M., Schwendiman, L. C., and Horst, T. W.: Aerosol transport in a naturally-convected boundary layer, Int. J. Heat Mass Trans., 15, 1837–1850, 1972.
- 10 Huang, S., Arimoto, R., and Rahn, K. A.: Sources and source variations for aerosol at Mace Head, Ireland, Atmos. Environ., 35, 1421–1437, 2001.
- Kalb, C. P., Dean, A. R., Peppler R. A., and Sonntag K. L.: Intercomparison of cloud base height at the ARM Southern Great Plains site, Presented 14th Atmospheric Radiation Measurement (ARM) Science Team Meeting, Albuquerque, NM, US Dept. of Energy, 2004.
- 15 Kunz, G., de Leeuw, G., Becker, E., and O'Dowd, C. D.: Lidar observations of atmospheric boundary layer structure and sea spray aerosol plumes generation and transport at Mace Head, Ireland (PARFORCE experiment), J. Geophys. Res., 107(D19), 8106, doi:10.1029/2001JD001240, 2002.
- Martucci, G. and O'Dowd, C. D.: Technical Report: ICOS field campaign at Mace Head, Ireland, June 2009.
- 20 Martucci, G., Matthey, R., Mitev, V., and Richner, H.: Comparison between backscatter lidar and radiosonde measurements of the diurnal and nocturnal stratification in the lower troposphere, J. Atmos. Ocean. Tech., 24, 1231–1244, 2007.
- Martucci, G., Milroy, C., and O'Dowd, C. D.: Detection of cloud-base height using Jenoptik CHM15K and Vaisala CL31 ceilometers, J. Atmos. Ocean. Tech., 2, 305–318, 2010a.
- 25 Martucci, G., Matthey, R., Mitev, V., and Richner, H.: Frequency of boundary-layer-top fluctuations in convective and stable conditions using laser remote sensing, Bound.-Lay. Meteorol., 135, 313–331, 2010b.
- McGovern, F. M., Krasenbrink, A., Jennings, S. G., Georgi, B., Spain, T. G., Below, M., and O'Connor, T. C.: Mass measurements of aerosol at mace head, on the west coast of Ireland, Atmos. Environ., 28, 1311–1318, 1994.
- 30 Mills, A. F. and Wassel, A. T.: Aerosol transport in a thermally driven natural convection boundary layer, Lett. Heat Mass Trans., 2, 159–167, 1975.

**Detecting boundary layer structure**

C. Milroy et al.

Münkel, C., Eresmaa, N., Rasanen, J., and Karppinen, A.: Retrieval of mixing height and dust concentration with lidar ceilometer, *Bound.-Lay. Meteorol.*, 124, 117–128, 2007.

Pearson, G., Davies, F., and Collier, C.: Remote sensing of the tropical rain forest boundary layer using pulsed Doppler lidar, *Atmos. Chem. Phys.*, 10, 5891–5901, doi:10.5194/acp-10-5891-2010, 2010.

Salma, I., Balásházy, I., Winkler-Heil, R., Hofmann, W., and Záray, G.: Effect of Particle mass size distribution on the deposition of aerosols in the human respiratory system, *J. Aerosol Sci.*, 33, 119–132, 2002.

Serafin, S. and Zardi, D.: Structure of the atmospheric boundary layer in the vicinity of a developing upslope flow system: a numerical model study, *J. Atmos. Sci.*, 67, 1171–1185, 2010.

Sicard, M., Molero, F., Guerrero-Rascado, J. L., Pedrós, R., Expósito, F. J., Córdoba-Jabonero, C., Rocadenbosch, F., Comerón, A., Pujadas, M., Alados-Arboledas, L., Martínez-Lozano, J. A., Díaz, J. P., Navas-Guzmán, F., and Gil, M.: Aerosol lidar intercomparison in the framework of SPALINET – the SPANish Lidar NETwork: methodology and results, *IEEE T. Geosci Remote*, 47, 3547–3559, 2009.

Stull, R. B.: *An Introduction to Boundary-Layer Meteorology*, Kluwer Academic Publishers, Dordrecht, 574–575, 666 pp., 1988.

Van Pul, W. A. J., Holtslag, A. A. M., and Swart, D. P. J.: A comparison of ABL heights inferred routinely from lidar and radiosondes at noontime, *Bound.-Lay. Meteorol.*, 68, 173–191, 1994.

Weitkamp, C.: *Lidar: Range-Resolved Optical Remote Sensing of the Atmosphere*, Springer Series of Optical Sciences, vol. 102, 460 pp., 2005.

Title Page	
Abstract	Introduction
Conclusions	References
Tables	Figures
◀	▶
◀	▶
Back	Close
Full Screen / Esc	
Printer-friendly Version	
Interactive Discussion	



## Detecting boundary layer structure

C. Milroy et al.

**Table 1.** Mean statistical parameters of the ALS300-CHM15K-CL31 intercomparison. For each  $X$  vs.  $Y$  comparison,  $R$  is the correlation coefficient, bias =  $\text{abs}(Y - X)$ , Sigma =  $\text{std}(Y - X)$ , consistency is percentage of  $X$  vs.  $Y$  detection closer than 200 m, i.e.  $\text{abs}(Y - X) \leq 200$  m.

	$R$	Bias (m a.g.l.)	Sigma (m a.g.l.)	Consistency (%)	Num. of cases
Comparison (SML)					
ALS300 vs. CHM15K	0.88	95.0	135.5	86.5	17
ALS300 vs. CL31	0.76	156.1	189.0	71.0	15
CHM15K vs. CL31	0.82	110.4	144.9	77.4	14
Comparison (DRCL)					
ALS300 vs. CHM15K	0.83	131.1	179.4	77.2	17
ALS300 vs. CL31	0.73	180.4	217.8	67.1	14
CHM15K vs. CL31	0.71	166.9	207.4	69.0	14

[Title Page](#)
[Abstract](#)
[Introduction](#)
[Conclusions](#)
[References](#)
[Tables](#)
[Figures](#)
[I◀](#)
[▶I](#)
[◀](#)
[▶](#)
[Back](#)
[Close](#)
[Full Screen / Esc](#)
[Printer-friendly Version](#)
[Interactive Discussion](#)


**Detecting boundary layer structure**

C. Milroy et al.

Title Page

Abstract

Introduction

Conclusions

References

Tables

Figures

I◀

▶I

◀

▶

Back

Close

Full Screen / Esc

Printer-friendly Version

Interactive Discussion

**Table 2.** List of backscatter data availability during the RS ascents.

RS [date, UTC]	CHM15K	CL31	ALS300
9 Jun 2009, 05:16	No data	X	X
9 Jun 2009, 11:40	No data	X	X
9 Jun 2009, 23:00	No data	X	X
10 Jun 2009, 05:30	rain	rain	rain
10 Jun 2009, 11:15	X	No data	X
10 Jun 2009, 17:00	X	No data	X
10 Jun 2009, 23:15	X	No data	X
11 Jun 2009, 05:00	X	No data	X
11 Jun 2009, 11:15	X	No data	X
11 Jun 2009, 17:15	X	No data	X
11 Jun 2009, 23:00	rain	rain	rain
12 Jun 2009, 05:30	rain	rain	rain
12 Jun 2009, 11:15	X	X	X
12 Jun 2009, 17:15	X	X	X
12 Jun 2009, 23:15	X	X	X
13 Jun 2009, 06:05	X	X	X
13 Jun 2009, 17:35	X	X	X
13 Jun 2009, 23:05	X	X	X
14 Jun 2009, 05:05	X	X	X
14 Jun 2009, 11:00	X	X	X
14 Jun 2009, 17:05	X	X	X
14 Jun 2009, 23:05	X	X	X
15 Jun 2009, 05:05	X	X	X

## Detecting boundary layer structure

C. Milroy et al.

**Table 3.** Mean statistical parameters of the ALS300-CHM15K-CL31 vs. Radiosounding (RS) comparison. For each  $X$  vs.  $Y$  comparison,  $R$  is the correlation coefficient,  $\text{bias}=\text{abs}(Y-X)$ ,  $\text{Sigma}=\text{std}(Y-X)$ , consistency is percentage of  $X$  vs.  $Y$  detections closer than 200 m, i.e.  $\text{abs}(Y-X)\leq 200$  m.

	$R$	Bias (m a.g.l.)	Sigma (m a.g.l.)	Consistency (%)	Num. of samples
Comparison (SML)					
ALS300 vs. RS	0.91	150.6	175.1	75.0	16
CL31 vs. RS	0.74	218.2	233.4	36.4	11
CHM15K vs. RS	0.88	177.2	191.6	64.7	17
Comparison (DRCL)					
ALS300 vs. RS	0.92	148.5	207.3	61.5	13
CL31 vs. RS	0.61	143.4	142.9	62.5	8
CHM15K vs. RS	0.81	192.1	235.8	53.3	15

[Title Page](#)
[Abstract](#)
[Introduction](#)
[Conclusions](#)
[References](#)
[Tables](#)
[Figures](#)
[I◀](#)
[▶I](#)
[◀](#)
[▶](#)
[Back](#)
[Close](#)
[Full Screen / Esc](#)
[Printer-friendly Version](#)
[Interactive Discussion](#)


## Detecting boundary layer structure

C. Milroy et al.

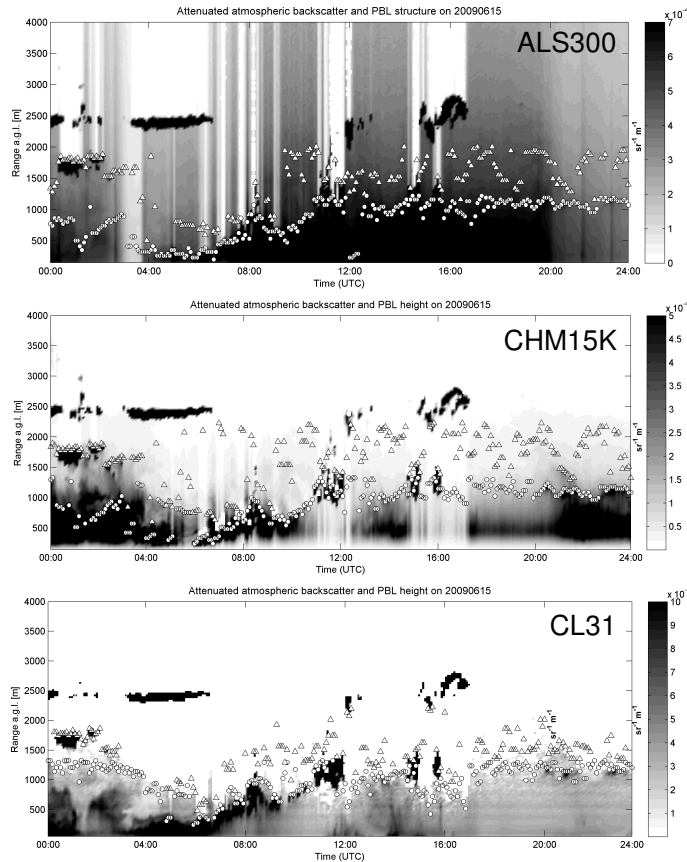


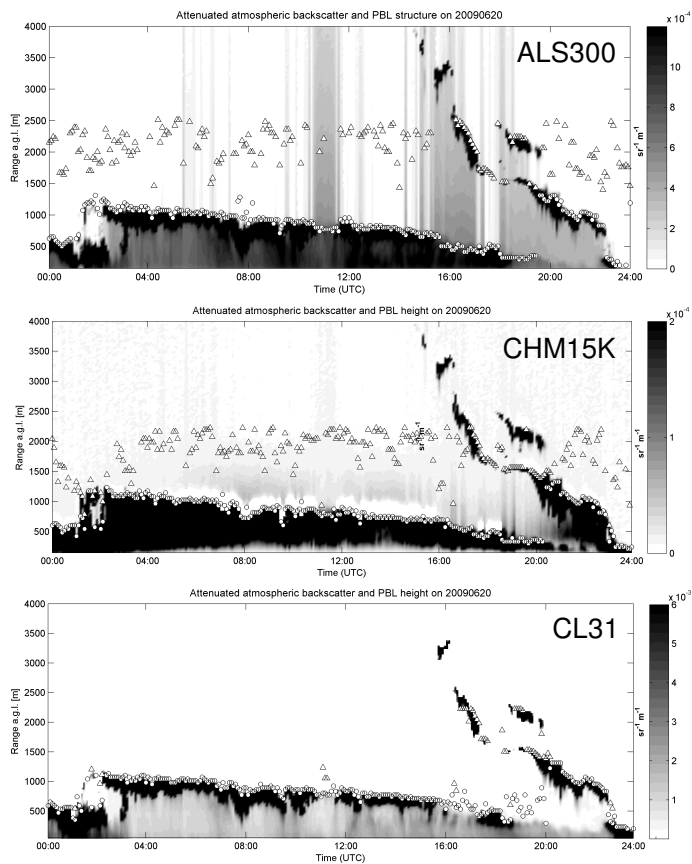
**Fig. 1.** Time-height cross sections of the atmospheric attenuated backscatter on 15 June 2009.

Title Page	
Abstract	Introduction
Conclusions	References
Tables	Figures
◀	▶
◀	▶
Back	Close
Full Screen / Esc	
Printer-friendly Version	
Interactive Discussion	



**Detecting boundary  
layer structure**

C. Milroy et al.

**Fig. 2.** Time-height cross sections of the atmospheric attenuated backscatter for 20 June 2009.

Title Page

Abstract

Introduction

Conclusions

References

Tables

Figures

◀

▶

◀

▶

Back

Close

Full Screen / Esc

Printer-friendly Version

Interactive Discussion



## Detecting boundary layer structure

C. Milroy et al.

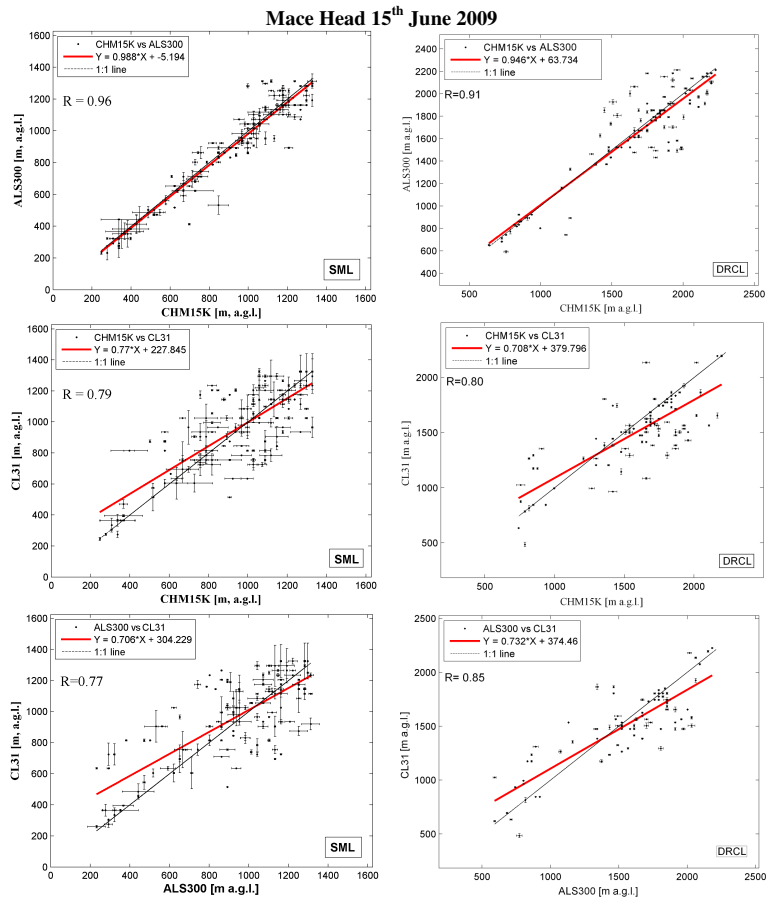


**Fig. 3.** Linear correlation for SML and DRCL detections on 15 June 2009. Upper left and right panels show the comparison ALS300 versus CHM15K; middle left and right panels show CL31 versus CHM15K; lower left and right panels show CL31 versus ALS300. A filter has been applied for outliers larger than two standard deviations ( $>2\sigma_{\text{stdv}}$ ).

[Title Page](#)
[Abstract](#)
[Introduction](#)
[Conclusions](#)
[References](#)
[Tables](#)
[Figures](#)
[⏪](#)
[⏩](#)
[⏴](#)
[⏵](#)
[Back](#)
[Close](#)
[Full Screen / Esc](#)
[Printer-friendly Version](#)
[Interactive Discussion](#)


## Detecting boundary layer structure

C. Milroy et al.

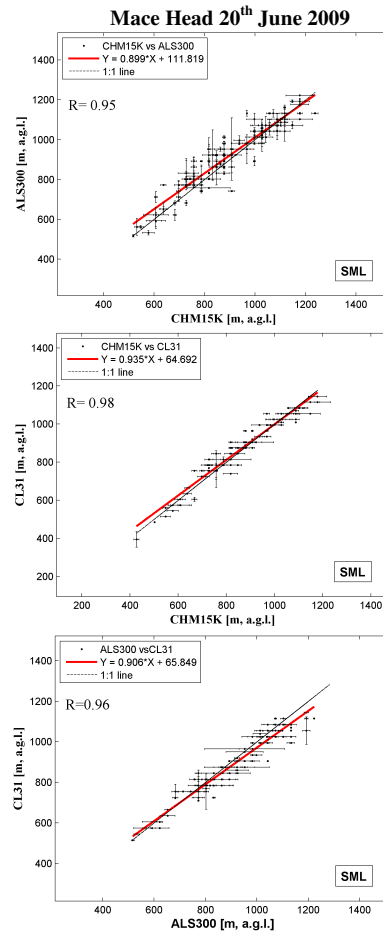


**Fig. 4.** Linear correlations of SML detections on 20 June 2009. Upper panel shows the comparison ALS300 versus CHM15K; middle panel shows CL31 versus CHM15K; lower panel shows CL31 versus ALS300. A filter has been applied for outliers larger than two standard deviations ( $>2\sigma_{\text{stdv}}$ ).

Title Page

Abstract

Introduction

Conclusions

References

Tables

Figures

◀

▶

◀

▶

Back

Close

Full Screen / Esc

Printer-friendly Version

Interactive Discussion



**Detecting boundary  
layer structure**

C. Milroy et al.

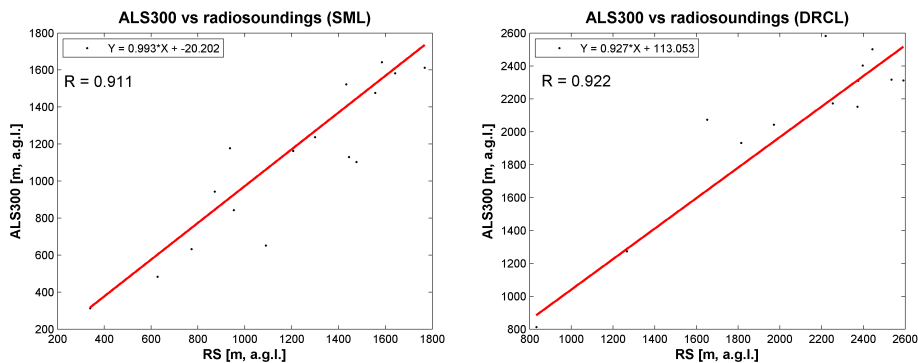


**Fig. 5.** ALS300 versus RS linear comparison and linear correlation for SML and DRCL detected heights.

Title Page

Abstract

Introduction

Conclusions

References

Tables

Figures

◀

▶

◀

▶

Back

Close

Full Screen / Esc

Printer-friendly Version

Interactive Discussion





**Detecting boundary layer structure**

C. Milroy et al.

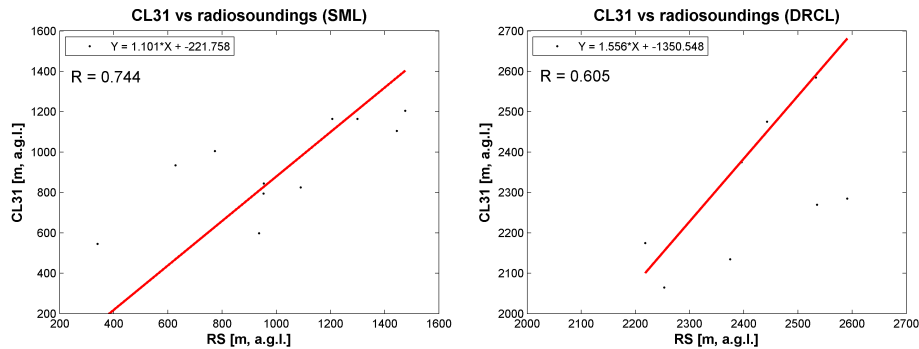


**Fig. 7.** CL31 versus RS linear comparison and linear correlation for SML and DRCL detected heights.

[Title Page](#)[Abstract](#)[Introduction](#)[Conclusions](#)[References](#)[Tables](#)[Figures](#)[◀](#)[▶](#)[◀](#)[▶](#)[Back](#)[Close](#)[Full Screen / Esc](#)[Printer-friendly Version](#)[Interactive Discussion](#)

**Detecting boundary layer structure**

C. Milroy et al.

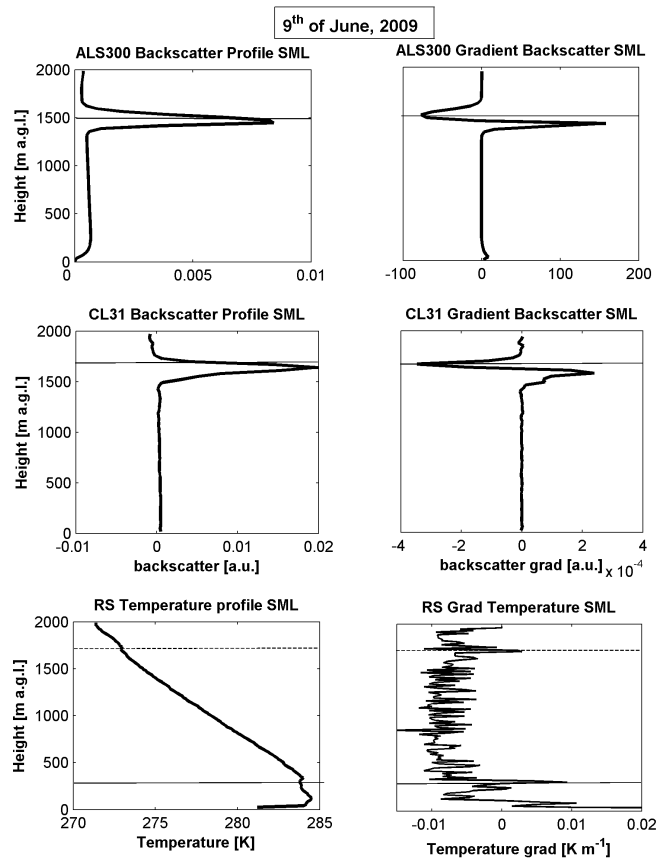


**Fig. 8.** Radiosoundings vs. CL31 and radiosoundings vs. ALS300 on 9 June 2009, 05:15 UTC. Top and middle left, 10-min averaged backscatter profile; top and middle right, log-gradient of backscatter profiles; bottom left, temperature profile; bottom right, vertical gradient of temperature profile. Horizontal dashed and solid lines represent DRCL and SML detection, respectively.

Title Page

Abstract Introduction

Conclusions References

Tables Figures

◀ ▶

◀ ▶

Back Close

Full Screen / Esc

Printer-friendly Version

Interactive Discussion



**Detecting boundary layer structure**

C. Milroy et al.

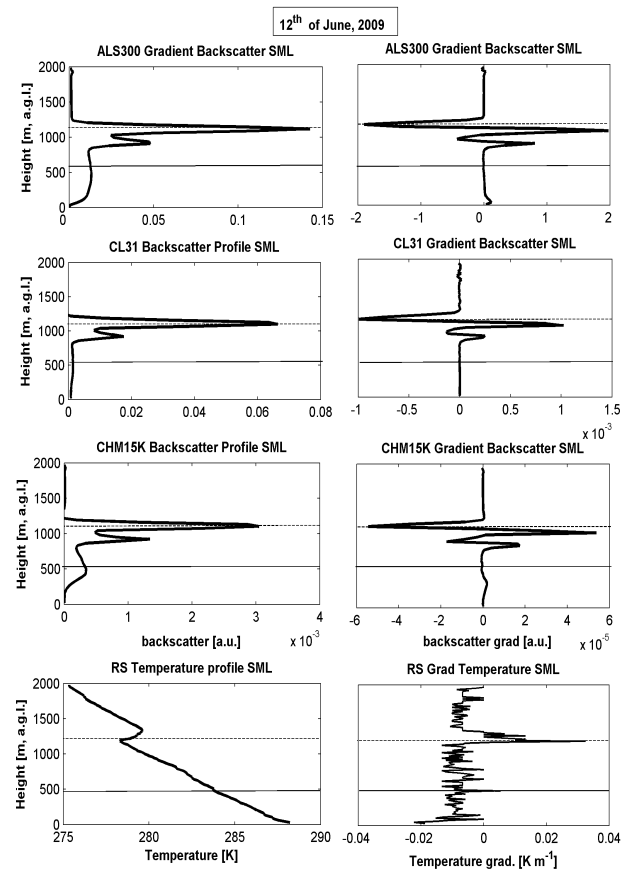


**Fig. 9.** Radiosoundings vs. CL31 and radiosoundings vs. ALS300 on 12 June 2009, 11:15 UTC. Top and middle left, 10-min averaged backscatter profile; top and middle right, log-gradient of backscatter profiles; bottom left, temperature profile; bottom right, vertical gradient of temperature profile. Horizontal dashed and solid lines represent DRCL and SML detection, respectively.

Title Page

Abstract Introduction

Conclusions References

Tables Figures

◀ ▶

◀ ▶

Back Close

Full Screen / Esc

Printer-friendly Version

Interactive Discussion

